4476 *Biochemistry* **2009,** *48,* 4476–4487
DOI:10.1021/bi8023509

BIOCHEMISTRY
including biophysical chemistry & molecular biology
Article

Crystal Structure of Baeyer−Villiger Monooxygenase MtmOIV, the Key Enzyme of the Mithramycin Biosynthetic Pathway[†,‡]

Miranda P. Beam,[§,⊥] Mary A. Bosserman,[§,⊥] Nicholas Noinaj,[∥,⊥] Marie Wehenkel,[§] and Jürgen Rohr*[,§]

[§]*Department of Pharmaceutical Sciences, College of Pharmacy, and Kentucky Center for Structural Biology, University of Kentucky, Lexington, Kentucky 40536, and* [∥]*Department of Molecular and Cellular Biochemistry and Kentucky Center for Structural Biology, University of Kentucky, Lexington, Kentucky 40536* [⊥]*These authors contributed equally to this work*

Received December 23, 2008; Revised Manuscript Received April 7, 2009

ABSTRACT: Baeyer−Villiger monooxygenases (BVMOs), mostly flavoproteins, were shown to be powerful biocatalysts for synthetic organic chemistry applications and were also suggested to play key roles for the biosyntheses of various natural products. Here we present the three-dimensional structure of MtmOIV, a 56 kDa homodimeric FAD- and NADPH-dependent monooxygenase, which catalyzes the key frame-modifying step of the mithramycin biosynthetic pathway and currently the only BVMO proven to react with its natural substrate via a Baeyer−Villiger reaction. MtmOIV's structure was determined by X-ray crystallography using molecular replacement to a resolution of 2.9 Å. MtmOIV cleaves a C−C bond, essential for the conversion of the biologically inactive precursor, premithramycin B, into the active drug mithramycin. The MtmOIV structure combined with substrate docking calculations and site-directed mutagenesis experiments identifies several residues that participate in cofactor and substrate binding. Future experimentation aimed at broadening the substrate specificity of the enzyme could facilitate the generation of chemically diverse mithramycin analogues through combinatorial biosynthesis.

Baeyer−Villiger monooxygenases (BVMOs)[1] were described and classified as a relatively new subclass of flavoprotein monooxygenases (*1*−*4*). BVMOs are powerful biocatalysts for synthetic organic chemistry applications (*5*−*7*), were also suggested to play key roles in the biosyntheses of various natural products (*8*−*13*), and are involved in prodrug activation (*14*, *15*) as well as in biodegradation reactions (*16*−*18*).

Mithramycin (MTM, also known as aureolic acid, mithracin, LA-7017, PA-144, and plicamycin) is an aureolic acid-type polyketide anticancer antibiotic produced by the soil bacterium *Streptomyces argillaceus* (ATCC 12956) and various other streptomycetes. The small distinct group of aureolic acid-type anticancer antibiotics includes MTM, chromomycin, olivomycin, UCH9, and durhamycin. All of these drugs contain the same polyketide-derived tricyclic aromatic core with a highly functionalized pentyl side chain attached at C-3 but vary with respect to their position 7 side chains and their saccharide patterns. MTM exhibits anticancer activity by inhibiting replication and transcription via cross-linking of DNA strands, affecting predominantly GC-rich regions normally used by Sp promoters (*19*−*23*). MTM has been used clinically to treat certain cancers, such as testicular carcinoma (*24*), and bone diseases, such as Paget's disease (*25*), and particularly to address cancer-related hypercalcemia (*26*). MTM was also recently identified as a lead drug for a potential therapy for Huntington's disease (*27*). However, the clinical use of MTM is currently limited because of its high toxicity, which potentially could be reduced with the generation of new analogues. MTM consists of a polyketide-derived tricyclic core with a highly functionalized pentyl side chain attached at position 3 and five deoxysugars linked as trisaccharide and disaccharide chains at positions 2 and 6, respectively (*28*) (Figure 1). The MTM biosynthesis (Figure 1) proceeds through the polyketide-derived tetracyclic premithramycinone, to which five sugar moieties and one C-methyl group at position 9 are added leading to premithramycin B (*29*). Then, MtmOIV oxidatively cleaves the fourth ring via a Baeyer−Villiger reaction, generating MTM's characteristic tricyclic aglycone core and highly functionalized pentyl side chain at position 3. The Baeyer−Villiger reaction precedes lactone opening, decarboxylation, and the final step of MTM biosynthesis, reduction of the 4′-keto group catalyzed by ketoreductase MtmW (*30*).

The function of MtmOIV as a BVMO was proven through studies with the isolated and overexpressed enzyme, allowing the isolation and characterization of key reaction intermediates, such as premithramycin B-lactone, the product mithramycin DK, and various shunt products (*31*).

[†]This work was supported by National Institutes of Health Grant CA 091901 to J.R.

[‡]The crystal data for MtmOIV were deposited in the Protein Data Bank (PDB) and have been assigned with the RCSB ID code rscb050786 and PDB entry 3FMW.

*To whom correspondence should be addressed. Phone: (859) 323-5031. Fax: (859) 257-7564. E-mail: jrohr2@email.uky.edu.

[1]Abbreviations: ASU, asymmetric unit; BVMO, Baeyer−Villiger monooxygenase; BV, Baeyer−Villiger; MOPS, 3-(*N*-morpholino)propanesulfonic acid; MTM, mithramycin; rmsd, root-mean-square deviation.

 Published on Web 4/13/2009

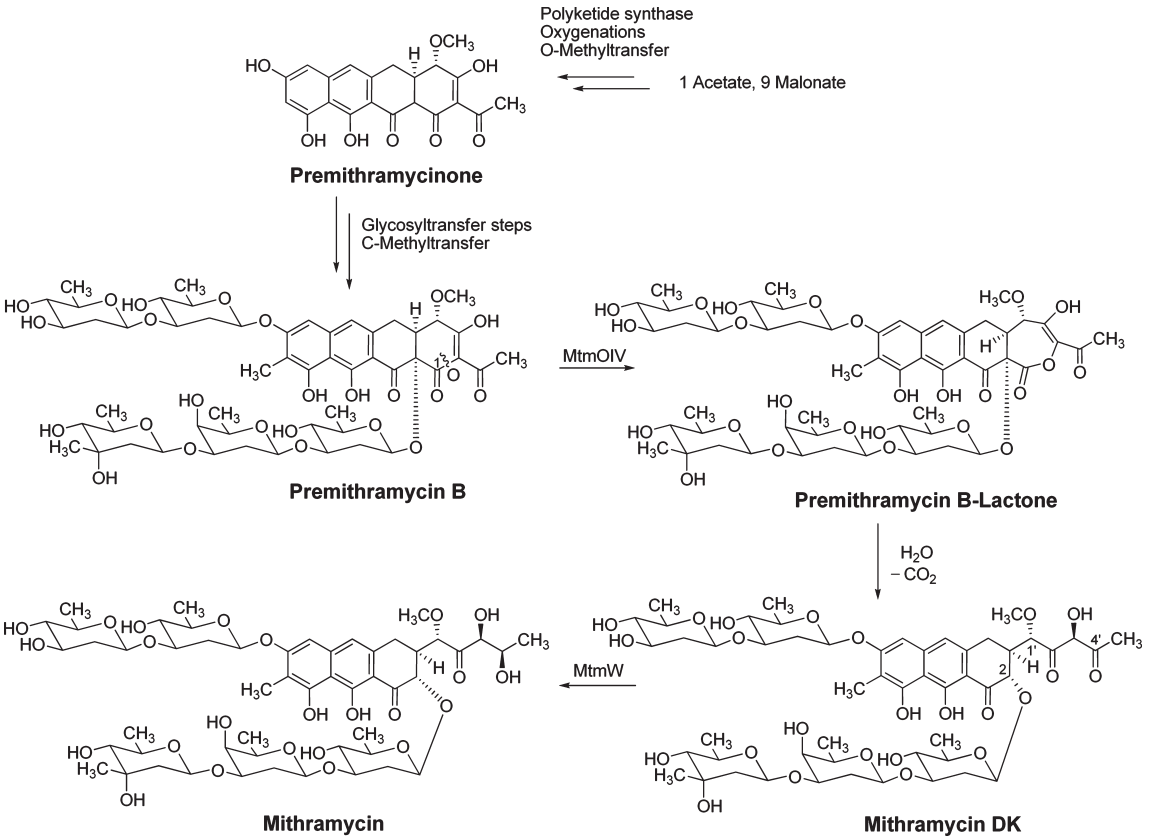

FIGURE 1: Biosynthetic pathway to mithramycin. The reaction catalyzed by BVMO MtmOIV yields premithramycin B-lactone, validating the BV mechanism, and premithramycin B-lactone is further converted to mithramycin DK (presumably spontaneously). The ketoreductase MtmW catalyzes the final step of mithramycin biosynthesis.

Only a few crystal structures of Baeyer−Villiger reaction-performing enzymes are available to date, including phenylacetone monooxygenase from the thermophilic bacterium *Thermobifida fusca* and the oxygenating component of 3,6-diketocamphane monooxygenase (*32*, *33*). Various BVMOs were described and studied, and most of these seem to be involved in oxidative degradation pathways, with substrates ranging from simple ketones, such as acetone or cyclohexanone, to steroids, such as progesterone (*34*, *35*). However, in many cases, it remains unclear whether the used substrates are the true natural substrates of such BV reaction-performing enzymes, and one could argue in several cases that the enzymes have no other choice but to perform a BV reaction when confronted with a relatively simple ketone substrate. In contrast, the MtmOIV substrate premithramycin B is a highly functional and decorated molecule and, so far, the most complex compound to date converted by a BV reaction. Thus, MtmOIV might be arguably the only BVMO that was investigated and kinetically characterized with its proven natural substrate (*31*, *36*−*38*).

Combinatorial biosynthesis produces new natural product drug analogues by recombining biosynthetic gene clusters with genes from other pathways and has been used recently to generate new MTM analogues, some with improved biological activities (*20*, *39*−*42*). Recent efforts were directed toward the design of new MTM analogues with altered saccharide patterns. However, despite some success, the number of such analogues is limited, partly due to restrictions imposed by the bottleneck enzyme MtmOIV, as the accumulation of various premithramycins suggested (*41*, *42*).

The crystal structure of MtmOIV was expected to provide insight into the intriguing enzymatic BV mechanism and pave the way for altering the substrate specificity of MtmOIV necessary for the generation of further mithramycin analogues. In its current state, MtmOIV appears to tolerate only some changes to the substrate, and compounds with a drastically altered, complete saccharide pattern cannot be converted and remain biologically inactive premithramycins. We hypothesized that if the binding properties of substrate premithramycin B in MtmOIV's active site were better understood, it would be feasible to engineer selected changes to residues involved in substrate binding, potentially leading to an enzyme with altered substrate specificity useful for the generation of further new bioactive analogues of MTM. To this end, we report here the crystal structure of MtmOIV, its putative substrate binding cavity, and residues likely involved in substrate binding.

On the basis of function and sequence similarity, MtmOIV was previously characterized as a member of the GR_2 subfamily of FAD-dependent enzymes (*37*, *43*). Recent additions to this family include PgaE and CabE, hydroxylases involved in angucycline biosynthesis pathways that have a high degree of sequence similarity (>45%) to MtmOIV. The crystal structures of PgaE and CabE were recently reported (*44*), and given the high level of sequence conservation, we were able to use these structures as models for molecular replacement. Previously, we reported the overexpression, crystallization, and preliminary structure determination of MtmOIV (*37*). Here, we present the refined 2.9 Å crystal structure of MtmOIV enabling characterization of the FAD binding site and identification of the putative substrate binding pocket. Mutations

to residues thought to be involved in FAD binding reduced the activity of the enzyme, as expected. Furthermore, cocrystallization and docking experiments with substrate premithramycin B provide some preliminary insight into the substrate binding, for which further evidence was gathered from selected mutations.

EXPERIMENTAL PROCEDURES

Protein Expression, Purification, and Crystallization. The cloning, overexpression, purification, crystallization, and initial data collection have previously been reported (*37*). Briefly, the *mtmOIV* coding sequence (1.5 kb) was amplified and subcloned into pRSETb and expressed with an N-terminal His_6 fusion tag for purification. This construct was then transformed into BL21(DE3)pLysS cells. A 1 L culture of NZCYM medium (Fisher) supplemented with 1 mM ampicillin and 1 mM chloramphenicol was grown at 37 °C until the OD_{600} reached 0.5−0.7, and then IPTG was added to a final concentration of 1 mM and the culture grown at 20 °C for an additional 12 h, which led to a higher protein yield of 14 mg/L of culture. Protein concentrations were determined by a Bradford assay (Sigma) for crystallization studies and a BCA assay (Pierce) for kinetic studies. Using a 1 mL well solution volume and drops consisting of 1 μL of protein and 1 μL of well solution, crystallization of MtmOIV was accomplished at room temperature using the hanging drop vaporization method with protein at 8 mg/mL and a well solution consisting of 0.1 M Na-HEPES (pH 7.5), 10% (v/w) PEG 8000, and 8% (v/v) ethylene glycol. The best crystals typically grew within 3−5 days, were harvested directly from the crystallization drop, and then were plunged into liquid nitrogen for storage until data collection. Cocrystallization was performed by preincubation of protein with premithramycin B (2:1 molar ratio with protein) for at least 1 h before crystallization trays were set.

Data Collection and Structure Determination. Crystals were initially screened using an in-house X-ray source (Rigaku Cu rotating anode X-ray generator, R-AXIS 4++ detector, CrystalClear software) with final data collected on the SER-CAT (ID-22) beamline at the Advanced Photon Source of the Argonne National Laboratory. The data were processed using HKL2000 (*45*) to space group *C*2 with the following cell dimensions: a = 145.27 Å, b = 114.44 Å, c = 138.56 Å, α = 90.00°, β = 103.03°, and γ = 90.00°. Initial cell content analysis using CCP4 (*46*) suggested four molecules per ASU with a solvent content of 51% (*37*). However, we observed only three molecules in the ASU, yielding a relatively high solvent content of 64%. Initial phases were determined by molecular replacement with PHASER within CCP4 (*46*) using PgaE (PDB entry 2QA1) as a search model where ClustalW (*47*) was used to create a sequence alignment between MtmOIV and PgaE which was then input into Chainsaw/CCP4 (*48*) to create an initial model. Model building was performed using PHENIX (*49*), and subsequent rebuilding and refinement, as well as water assignments, were performed using COOT(*50*), CNS (*51*), and PHENIX (*49*) with restrained NCS averaging and TLS refinement. The final structure of MtmOIV was refined to 2.9 Å resolution with final R and R_{free} values of 0.24 and 0.29, respectively, with 494 of 533 residues. The N-terminal His_6 tag was not observed within the crystal structure and assumed to be disordered since it was not removed during purification. The final structure was analyzed using Molprobity (*52*), and figures were created using PyMOL (*53*). rmsd analysis was performed using STRAP (*54*).

MtmOIV Mutagenesis. The putative FAD binding site mutants F180A and F272A were prepared and analyzed (Table 2). Due to high GC content (>80%), the Stratagene QuikChange kit was utilized with primers designed for site saturation (*55*) with a slow down PCR technique incorporated in the design of the temperature cycles (*56*). The mutagenesis primers used for F180A were (forward) 5′-GAT CGG GCT CCC-GGC ACC GAG GCC ACC GTC CGC GCC-3′ and (reverse) 5′-GGT GCC GGG AGC CCG ATC CGA GGC CAG CCG-CCA CAC-3′ and for F272A were (forward) 5′-TCC CGG GCA-GGA GAC GCG AGC CGC CAG GCG AAG CGC TAC-3′ and (reverse) 5′-CGC GTC TCC TGC CGC GGA GAG CCA-CGA CAC CGA TTC-3′. Substrate binding site mutants and R52A were prepared with the Stratagene QuikChangeXL kit following the standard protocol. Mutagenesis primers used for F89A were (forward) 5′-C TTC GCC GGG ATC GCC ACC-CAG GGC CTG-3′ and (reverse) 5′-CAG GCC CTG GGT-GGC GAT CCC GGC GAA G-3′, for L107A were (forward) 5′-C CCG TAC ACG GGC GCG GTG CCG CAG TCG-3′ and (reverse) 5′-CGA CTG CGG CAC CGC GCC CGT GTA CGG-G-3′, for R204A were (forward) 5′-GAG GTG CCG CGC GCC-TGG GAG CGC AC-3′ and (reverse) 5′-GT GCG CTC CCA-GGC GCG CGG CAC CTC-3′, and for R52A were (forward) 5′-C GGC CAC GAC GCG GCG GGG GCC-3′ and (reverse) 5′-GGC CCC CGC CGC GTC GTG GCC G-3′.

FAD Content. Each protein preparation of wild-type and mutant MtmOIV enzymes contained noncovalently bound FAD molecules demonstrated by the bright to faint yellow color of the preparations following purification. The concentration of FAD was determined using a Shimadzu UV-1800 spectrophotometer. Initially, approximately 100 μg of protein (100 μL) was diluted 1:3 in 20 mM potassium phosphate (pH 8.25), and 25 μL of 50% trichloroacetic acid (TCA, Fisher) was added to bring the final concentration of the solution to 3% TCA. The protein was precipitated on ice for 30 min and spun at 10000*g* for 5 min. The supernatant was removed, and its absorbance was measured. The FAD content was determined by absorbance at 450 nm (ε_{450} = 11300 M^{-1} cm^{-1}).

Kinetic Analysis of MtmOIV. A kinetic assay has been previously reported (*31*). Briefly, we monitored the conversion (pH 8.25, 30 °C, 10 min) of premithramycin B by MtmOIV in a continuous assay measuring the oxidation of NADPH at 340 nm (ε_{340} = 6220 M^{-1} cm^{-1}) in the presence of FAD and O_2 (0.25 mM NADPH/NADH; 0.1 mM FAD added; open cuvette). The reactions were initiated by addition of 1 μM wild type or mutant MtmOIV. Kinetic parameters were determined by fitting with Kaleidagraph 4.0 (Synergy).

Uncoupling Assays. To estimate reaction uncoupling, production of hydrogen peroxide was measured. At the termination of a 10 min kinetic reaction (1 μM enzyme, 102 μM substrate, 250 μM NADPH, 100 μM FAD, open cuvette), a 100 μL sample was withdrawn and used in the following assay. Briefly, 700 μL of 5 mM 4-aminoantipyrene, 10 mM vanillic acid, and 40 units/mL horseradish peroxidase in 0.2 M sodium chloride and 0.2 M MOPS (pH 7.5) was combined with 100 μL of enzyme reaction mixture. In this assay, horseradish peroxidase uses hydrogen peroxide to oxidize 4-aminoantipyrene, creating a product that condenses with vanillic acid to produce a red quinone imine dye. The dye has a broad absorbance spectrum peaking at ~490 nm. A 30% (w/w) H_2O_2 stock (Mallinckrodt) was used to create a

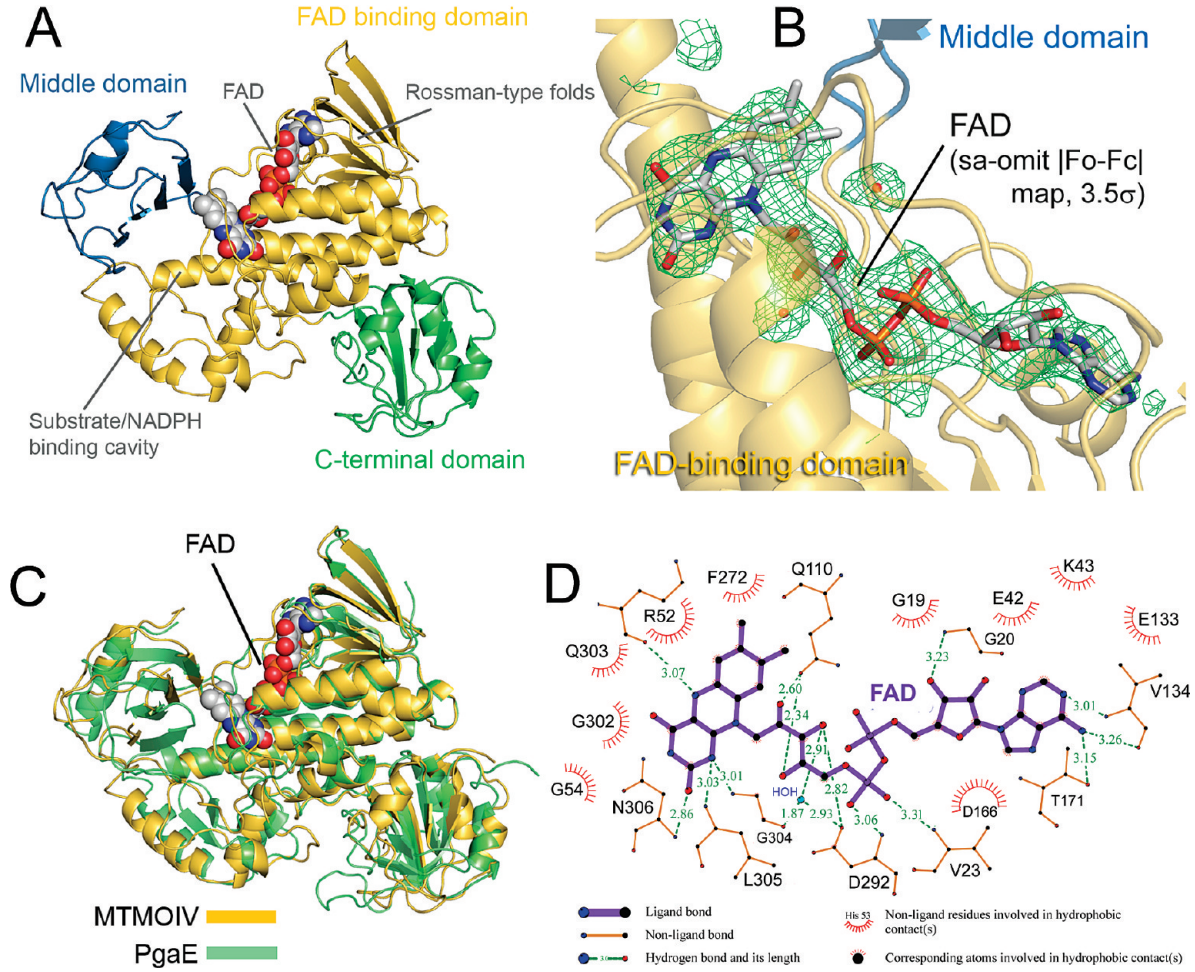

FIGURE 2: (A) Overall structure of MtmOIV. The FAD binding domain is colored gold, the middle domain blue, and the C-terminal domain green. The FAD cofactor is shown as spheres. The Rossman-type fold and the substrate/cofactor binding cavity are indicated accordingly. (B) View of FAD binding with FAD shown in stick format and simulated annealing omit $|F_o - F_c|$ electron density (3.5σ) for FAD in green mesh. The FAD binding domain is colored gold and the middle domain blue. (C) Superposition of the crystal structures of MtmOIV (gold) and PgaE (green). The FAD cofactor is shown as spheres. (D) FAD binding with involved residues and distances. This figure was created using LIGPLOT (*62*).

standard curve from 0 to 1 mM, and the absorbance at 490 nm was measured to determine the hydrogen peroxide content in reaction samples (*57*, *58*).

Premithramycin B Docking Experiments. The structure of premithramycin B was created using the PRODRG2 Server (*59*, *60*), and docking experiments were performed using AutoDock 4 (*61*) and an Autogrid starting location based on difference density observed in a low-resolution cocrystal structure from a MtmOIV−premithramycin B cocrystallization attempt (data not shown).

RESULTS

Overall Structure. MtmOIV crystallized in space group *C*2. The structure was refined to a resolution of 2.9 Å with three molecules in the asymmetric unit. The final structure contains residues 14−508 of 533 total residues for MtmOIV, including the FAD cofactor (Figure 2A). The FAD cofactor was found noncovalently bound in the crystal structure (Figure 2B). Additionally, the N-terminal His_6 tag used for purification and the last 25 residues of the C-terminus were found to be disordered, and not present. Approximately 15% of the side chains were not visible in the electron density maps and were therefore left out of the final structure. This observation is likely attributed to both the high solvent content of the crystals (64%) and the low resolution of the crystal structure. There is an absent loop along residues 218−226 in the MtmOIV structure which corresponds to a previously reported disordered surface loop in PgaE, likely attributed to mobility and shown to be involved in the association with NADPH (*44*), which also is a cofactor of MtmOIV.

As expected, on the basis of a high level of sequence identity (~43%), the structure of MtmOIV is very similar to the structure of PgaE with an rmsd of 2.38 Å for 463 aligned residues (Figure 2C). In total, 98.3% of the MtmOIV residues were in the Ramachandran allowed regions with 78% in the most favored regions. Final data collection and refinement statistics are summarized in Table 1. Figure 2A shows that MtmOIV contains three domains: the FAD binding domain (residues 14−183 and 276−394), the middle domain (residues 184−275), and the C-terminal domain (residues 395−508). The FAD binding domain contains two Rossman-like $\beta\alpha\beta$ folds (G19−G24 and G162−G167) and forms the central hub of the enzyme's structure.

Within MtmOIV, FAD can potentially adopt one of two structural conformations (IN or OUT) on the basis of the solvent accessibility of the moiety and its orientation toward the putative substrate binding pocket. In contrast to the current literature, the FAD cofactor appears to be stabilized in the IN conformation. Thirteen direct hydrogen bonds could be identified within the binding pocket stabilizing the FAD moiety and promoting

Table 1: MtmOIV Data Collection and Refinement Summary

space group	*C*2
no. of molecules per asymmetric unit	3
λ (Å)	1.0
Matthew's coefficient	3.91
solvent content (%)	68.34
a (Å)	145.24
b (Å)	114.48
c (Å)	138.61
α (deg)	90.00
β (deg)	103.03
γ (deg)	90.00
resolution (Å)[a]	2.9−30 (2.9−3.0)
completeness (%)[a]	96.3 (91.7)
redundancy[a]	3.5 (2.5)
R_{sym}[a,b]	6.8 (46.1)
I/σ[a]	22.4 (2.1)
R^c/R_{free}[d]	0.24/0.29
no. of unique reflections	47403
Wilson *B*-factor (Å^2)	79.08
average *B*-factor (Å^2)	92.3
rmsd for bond lengths (Å)	0.005
rmsd for bond angles (deg)	0.908
no. of water molecules	6
Ramachandran plot	
most favored region (%)	78.0
additionally allowed region (%)	17.3
generously allowed region (%)	3.0
disallowed region (%)	1.7
PDB entry	3FMW

[a] Statistics in the last resolution shell shown in parentheses. [b] $R_{sym} = \sum_{hkl,j}(|I_{hkl} - \langle I_{hkl}\rangle|)/\sum_{hkl,j} I_{hkl}$, where $\langle I_{hkl}\rangle$ is the average intensity for a set of *j* symmetry-related reflections and $\langle I_{hkl}\rangle$ is the value of the intensity for a single reflection within a set of symmetry-related reflections. [c] *R*-factor = $\sum_{hkl}(||F_o| - |F_c||)/\sum_{hkl}|F_o|$, where F_o is the observed structure factor amplitude and F_c is the calculated structure factor amplitude. [d] $R_{free} = \sum_{hkl,T}(||F_o| - |F_c||)/\sum_{hkl,T}|F_o|$, where a test set, T (5% of the data), has been omitted from the refinement.

solvent inaccessibility to the FAD molecule (Figure 2B,D). R52A is involved in a hydrophobic interaction and a hydrogen bond interaction (3.07 Å) with the isoalloxazine ring of FAD. These interactions place R52 in a reasonable position to perform its chemistry. With RebC, it was recently demonstrated that FAD adopts an IN conformation when substrate is bound or FAD is reduced and remains in an OUT conformation in substrate-free and nonreduced FAD states (*63*). Although a secondary structure of MtmOIV in the substrate-bound state is needed to confirm the orientation of FAD, from this single-state structure, FAD appears to be in the IN conformation.

In the structural alignment, the elements are numbered the same as PgaE for reference (Figure 3). MtmOIV is a known dimer (Figure 4) in solution (*37*), and the dimer interface can be observed within the crystal structure, stretching along both the FAD binding domain (involving residues R345, L348, N349, R351, A352, L354, A355, L356, R358, D360, E361, Q362, H363, T364, P366, L367, F370, E373, L374, T377, E379, Y383, F384, and M387) and the middle domain (involving residues T183, E184, T186, V187, T232, and D274). Using the PISA Server (*64*), the buried surface area between the dimers was calculated to be ~1200 Å^2, which is ~5.7% of total surface area for each monomer.

Cofactor Binding. To further probe the FAD binding site, interactions with residues F180 and F272 were tested by mutation of these residues to alanine. Both phenylalanine residues seem to be involved only in more or less distant hydrophobic and/or steric interactions with the aromatic rings of FAD. F272 appears to interact with the isoalloxazine moiety of FAD and F180 rather distantly with FAD's adenine moiety. Thus, both mutations were designed to decrease the level of FAD binding, but not to completely inactivate the enzyme (Figure 5A). Unfortunately, FAD binding was not maintained with these mutations, activity almost completely lost, and turnover so limited that kinetic and catalytic parameters were not able to be determined within the substrate concentration range tested, up to 200 μM (Table 2). Kinetic activity was compared to that of the native enzyme by monitoring the oxidation of the NADPH cofactor in the presence of FAD and O_2.

Substrate Binding. The substrate binding site for MtmOIV was partially identified by a low-resolution (3.6 Å) crystal structure from an MtmOIV−premithramycin B cocrystallization experiment (data not shown). While difference density, presumably for premithramycin B, was observed in the cocrystal structure when compared to the native structure, the density was poor and not large enough to accommodate the entire ligand, possibly due to disorder in the structure of the compound, the low resolution of the crystal structure, and/or the low occupancy in the crystal structure (Figure 6). Since we could not determine the interactions between MtmOIV and premithramycin B directly from the crystal structure, we used the partial information gathered from the difference density in the cocrystal structure, along with what is already known about FAD-dependent enzymes, to estimate a starting location for modeling premithramycin B into the MtmOIV crystal structure using Autodock 4 (*61*). An Autogrid template was centered along the region of observed difference density in our crystal structure, and the cluster of conformations with the lowest docking energy was analyzed to determine the best docking solution.

The estimated free energy of binding for premithramycin B was −3.57 kcal/mol, which is within acceptable limits (*65*). Other Autodock model data statistics were as follows: estimated K_i = 2.41 mM, final intermolecular energy = −6.04 kcal/mol, vdW + H-bond + desolvation energy = −5.88 kcal/mol, electrostatic energy = −0.17 kcal/mol, final total internal energy = −6.24 kcal/mol, torsional free energy = +5.76 kcal/mol, and unbound system's energy = −2.95 kcal/mol. The modeled substrate sits in the putative active site cleft (Figures 5B and 7A) and suggests an ~5.3 Å distance between C1 of premithramycin B and C4a of FAD, to which the hydroperoxy group is known to be bound (Figures 2A and 7B). This distance agrees well with reports of other FAD-dependent enzymes, the distance typically ranging between 4.5 and 5.5 Å (*66*). It is known that the FAD cofactor is essential for the enzyme function within the GR_2 subclass (*43*) of FAD-dependent enzymes and that FAD's role is to transfer an oxygen molecule from O_2 to the premithramycin B, subsequently releasing H_2O (*36*). Therefore, the FAD binding site must be in the proximity of the enzyme's active site for the oxygen transfer, which is consistent with the observations of our modeling studies.

To gather supporting evidence for the suggested substrate binding site, we generated mutants F89A, L107A, and R204A. Figure 5B shows these three residues are possibly involved in substrate binding through interactions with the tetracyclic aglycone (L107) and the mycarose moiety (sugar E) of the trisaccharide chain (F89 and R204), respectively, of premithramycin B. The latter two of these three selected residues seem distant from the FAD binding site, and although an effect on FAD binding is possible, the mutations should more directly affect substrate binding.

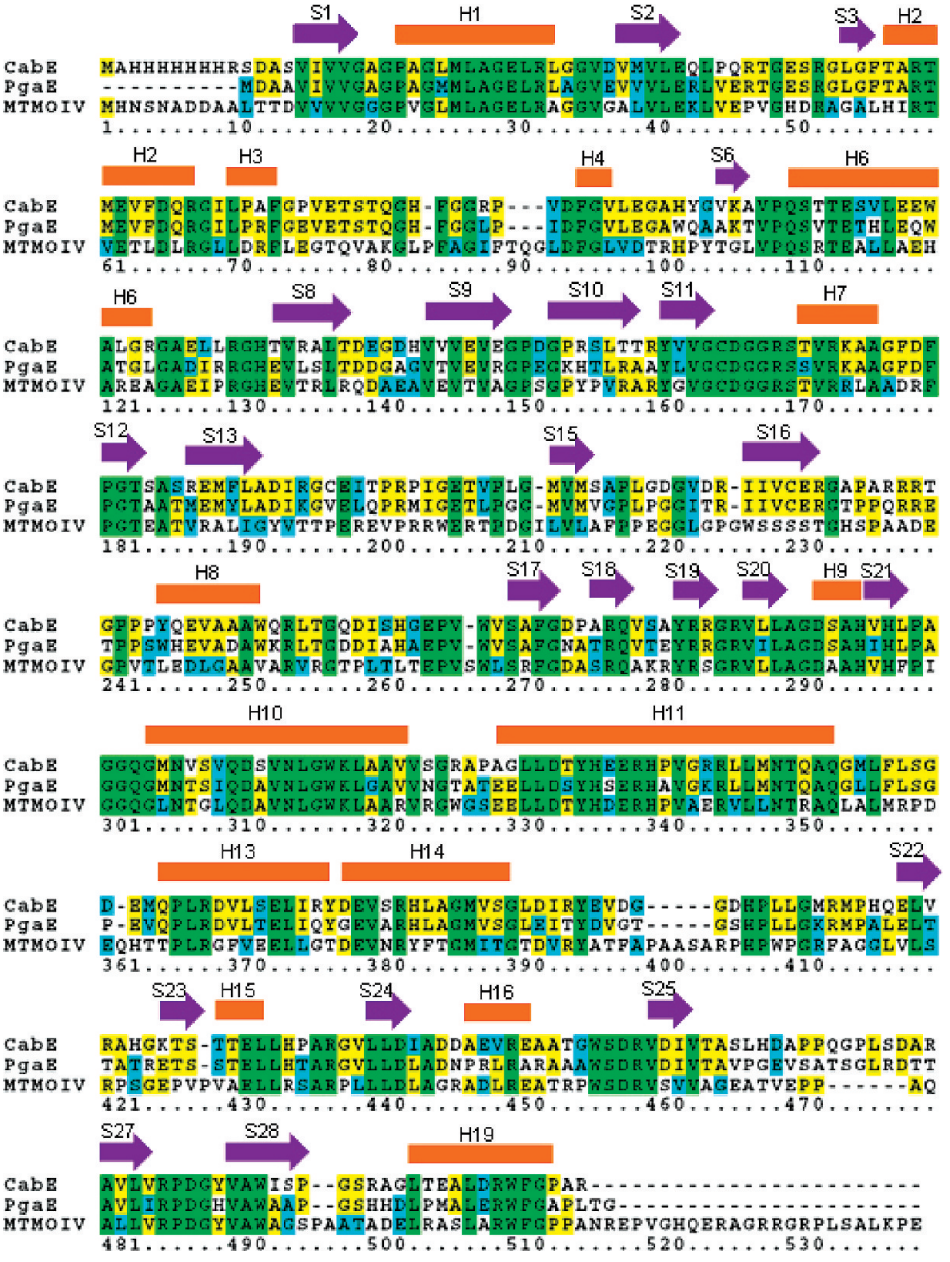

FIGURE 3: Sequence alignment of MtmOIV, PgaE, and CabE. Green shading indicates residues that are completely conserved, yellow residues that are partially conserved, and cyan residues that are similar. Secondary α-helix structures are labeled as orange blocks above the residues and β-sheets with purple arrows. Structural labels have the same numbering as the PgaE structure (*44*).

Steady State Kinetics. Enzymatic turnover was correlated with the consumption of NADPH and calculated by measuring the decrease in absorption at 340 nm (ε_{340} = 6220 M^{-1} cm^{-1}). Kinetic parameters were determined for each of the enzymes. The K_m for wild-type MtmOIV was similar to previous reports of 31 μM (*31*, *36*). In contrast, the V_{max} (966 nmol min^{-1} mg^{-1}) of MtmOIV was significantly increased and is attributed to higher concentrations of NADPH in the assay, 0.25 mM compared with 0.1 mM. Kinetic analysis of the FAD and substrate binding site mutants confirms an important dependency on FAD binding. Of the six mutant enzymes, three (L107A, F180A, and F272A) were extremely deficient in FAD binding with undetectable levels of FAD as measured by absorbance at 450 nm. The FAD deficiency translated into enzymatic inefficiency. Each of these enzymes had impaired kinetics with NADPH consumption curves lacking any initial fast phase. Even at substrate concentrations 3-fold greater than K_m (102 μM premithramycin B), these three enzymes exhibited marginally detectable activity.

Two substrate binding site mutants (F89A and R204A) and a mutant (R52A) aimed at destabilizing an intermediate of the BVMO reaction mechanism maintained varying amounts of FAD binding (Table 2). From the purification experiments, it seems that wild-type MtmOIV binds approximately one FAD cofactor per two enzyme monomers, F89A has similar FAD content, and R204A binds approximately half the FAD of the wild type and F89A. R52A has 8-fold lower FAD content than the wild-type enzyme and also shows the greatest reduction in activity of the three mutants. R52A activity is reduced by >10-fold (comparison of k_{cat}/K_m values between the two enzymes). The increase in K_m (R52A, 79 μM) from the wild-type value suggests an additional consequence of the mutation aside from FAD content reduction. Inefficiency at stabilizing a reaction intermediate or a reduced affinity for the initial substrate could

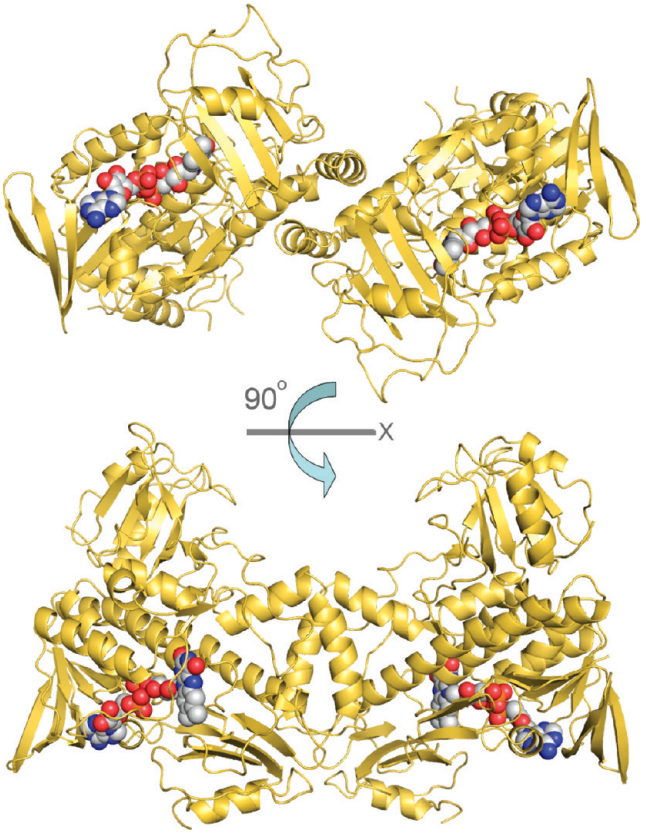

FIGURE 4: Biological subunit of MtmOIV as a dimer, which has ~1200 Å^2 of buried surface area (5.7% of the total surface area for each monomer) which is mediated along the FAD binding domain and the middle domain.

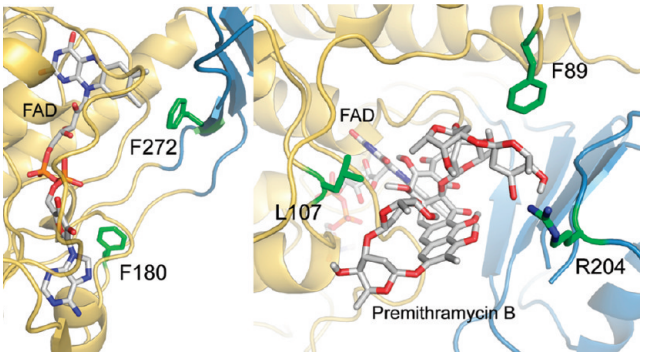

FIGURE 5: (A) Residues F180 (green), close to the adenine moiety of FAD, and F272 (green), close to the isoalloxazine moiety of FAD (gray stick with N atoms colored blue, O atoms red, and P atoms orange), were selected for mutagenesis to support the FAD binding area in MtmOIV (gold/blue ribbon). (B) Residues L107, R204, and F89 (all colored green) were chosen to support their involvement in substrate (premithramycin B, gray stick, with O atoms colored red) binding. The isoalloxazine moiety of FAD (gray stick with N atoms colored blue, O atoms red, and P atoms orange) and the enzyme are shown in gold/blue ribbons. The results (Table 2) show that residues F89 and R204 possibly constrict the premithramycin B binding site, while the L107A mutation reduces the level of substrate binding, and also FAD binding.

explain the altered kinetics of R52A. Clearly, the mutation negatively affects the kinetics of MtmOIV.

Both F89A and R204A mutants maintain high FAD content compared to the other mutants, and the activity of these two enzymes is increased from the wild-type value, with k_{cat}/K_m values of 47 and 41 s^{-1} mM^{-1}, respectively, compared to 35 s^{-1} mM^{-1} for the wild type. Each enzyme accomplishes this increase through a distinct mechanism. While F89A has a K_m comparable to that of the wild type and a significantly increased k_{cat} value, R204A has a comparable k_{cat} but a decreased K_m, effectively heightening the activity of each mutant with respect to that of the wild type.

In addition to NADPH, NADH is also a functional coenzyme in the MtmOIV reaction mechanism; however, the exact kinetic parameters have not yet been defined (*36*). Within error, we found a similar K_m in the presence of 0.25 mM NADH, but k_{cat} was decreased, limiting the k_{cat}/K_m value to ~70% of that of the wild-type enzyme with NADPH as the cofactor.

DISCUSSION

The structure of BVMO MtmOIV has been determined, revealing many similarities with other characterized FAD-dependent enzymes. The structure contains an FAD molecule noncovalently bound adjacent to a large substrate binding cavity which is able to perfectly accommodate the substrate premithramycin B. Bordering this cavity is MtmOIV's active site, including the flavin ring of the FAD cofactor, which is required for catalysis.

MtmOIV does have a novel structure for a BVMO compared to the only so far published structures of BVMOs, namely, phenylacetone monooxygenase (PAMO) from the thermophilic bacterium *T. fusca* (PDB entry 1W4X) (*33*, *67*) and 3,6-diketocamphane monooxygenase from *Pseudomonas putida* (by comparison with the shown structure, which is not deposited in the PDB) (*32*). PAMO has significant differences compared to MtmOIV with an rmsd of 5.78 Å for only 282 aligned residues. The differences may be explained by the enzyme substrates which are vastly different in size, although the native functionality of phenylacetone monooxygenase in *T. fusca* is unknown. However, there are also similarities regarding the active site. Most importantly, MtmOIV possesses, like PAMO, an arginine residue (Arg-52) that is located above the flavin ring (Figure 8A), suited to stabilize both the negatively charged peroxyflavin and Criegee intermediates involved in the BV reaction mechanism (*1*, *2*, *33*). However, while the corresponding R337 of PAMO is located on the *re* side of the flavin ring (*33*), R52 of MtmOIV lies on the *si* side (Figure 8A).

Nevertheless, the overall mechanism of the initial MtmOIV reaction (for the likely sequence of events, see Figure 8B) should be similar as described for PAMO (*33*), and R52 should play a similar important role for MtmOIV as R337 for PAMO. Thus, R52 mutagenesis was expected to significantly decrease the rate of enzyme turnover by interfering with crucial interactions between the enzyme and reaction intermediates. Indeed, mutant enzyme R52A's efficiency [13% of that of the native enzyme (see Table 2)] decreased significantly but did not render the enzyme inactive, possibly indicating a compensatory mechanism of intermediate stabilization. In contrast, the analyzed R337A and R337K mutants of PAMO, while still able to form and stabilize the C-4a-peroxyflavin intermediate, were unable to convert the substrate phenylacetone (*67*). However, since we monitored the oxidation of NADPH, the activity of the R52A mutant found remaining might also point to a biosynthetic shunt pathway, through which NADPH is oxidized, e.g., an NADPH-triggered reduction of premithramycin B. We are hopeful future studies on MtmOIV will clarify some of these mechanistic questions.

MtmOIV and PgaE are highly similar both in sequence and in structure, as seen in Figures 2C and 3. However, the reactions they

Table 2: Comparison of Activity of MtmOIV, Substrate Binding Site Mutants F89A, L107A, and R204A (blue), and FAD Binding Site Mutants F180A, F272A, and R52A (red) versus That of the Wild-Type Enzyme (WT) Using NADPH (preferred) or NADH (less preferred) as a Cofactor

	K_m (μM) for PreB	k_{cat} (s^{-1})	k_{cat}/K_m (s^{-1} mM^{-1})	FAD mole ratio (mol of MtmOIV/mol of FAD)	uncoupling ratio (102 μM PreB, 10 min) (mol of product/mol of H_2O_2)
			NADPH		
WT	31 ± 10	1.10 ± 0.11	35	0.56	15
F89A	27 ± 9	1.27 ± 0.11	47	0.42	> 80
L107A	–	–	–	< 0.01	–
R204A	18 ± 3	0.73 ± 0.02	41	0.24	> 300
R52A	79 ± 10	0.21 ± 0.01	2.7	0.07	> 50
F180A	–	–	–	< 0.01	–
F272A	–	–	–	< 0.01	–
			NADH		
WT	38 ± 18	0.97 ± 0.14	26	0.56	–

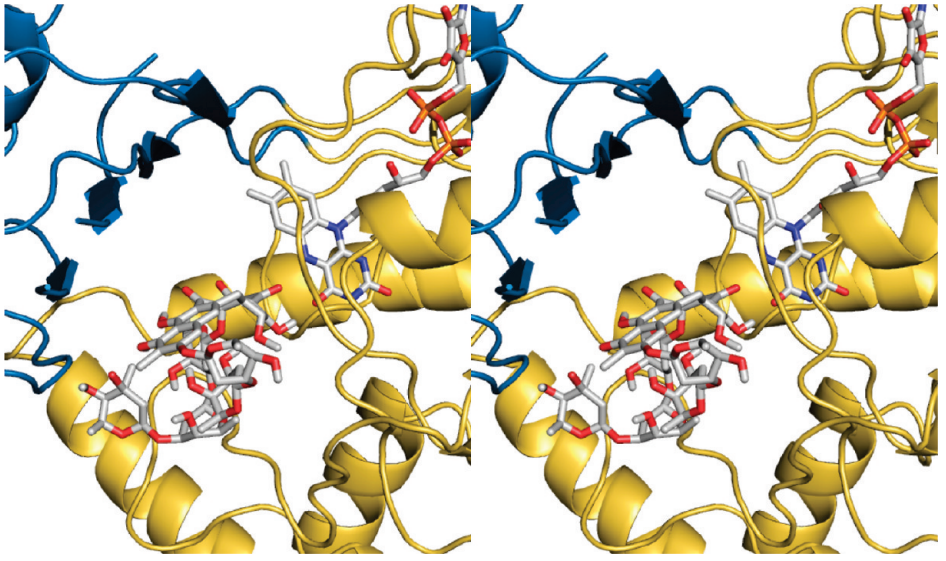

FIGURE 6: Stereoimage of the premithramycin B (gray stick) binding pocket with FAD (gray stick), based on the found density from premithramycin B−MtmOIV cocrystallization and initial Autodock computational studies, prior to refinement (for the Autodock-refined results, see Figures 5B and 7) . MtmOIV is shown as a gold (FAD binding domain) and blue (middle domain) ribbon.

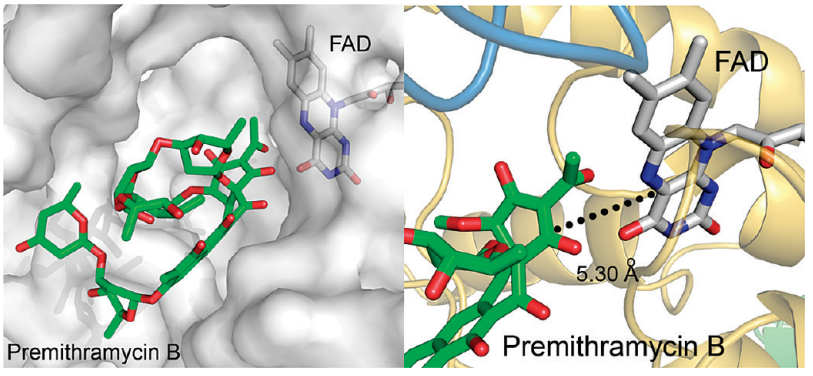

FIGURE 7: (A) Premithramycin B (green stick) binding pocket with FAD (gray stick). MtmOIV is shown in transparent gray surface representation. (B) The dotted line represents the measured distance of 5.30 Å from C4a of the flavin ring of FAD to C1 of premithramycin B.

catalyze are fundamentally different, although both are post-polyketide synthase tailoring enzymes. PgaE is an aromatic hydroxylase isolated from a cryptic gene cluster from *Streptomyces* sp. PGA64 involved in angucycline biosynthesis, catalyzing the C12 hydroxylation of UWM6 as an early post-PKS tailoring step toward gaudimycin C (Figure 9) (*68*), which is mechanistically an electrophilic aromatic substitution reaction, while MtmOIV is a Baeyer−Villiger monooxygenase involved in the biosynthesis of the aureolic acid class anticancer agent mithramycin, which initiates its reaction sequence through a nucleophilic attack of one of the four keto functions of premithramycin B (Figures 1 and 8B) (*31*, *38*).

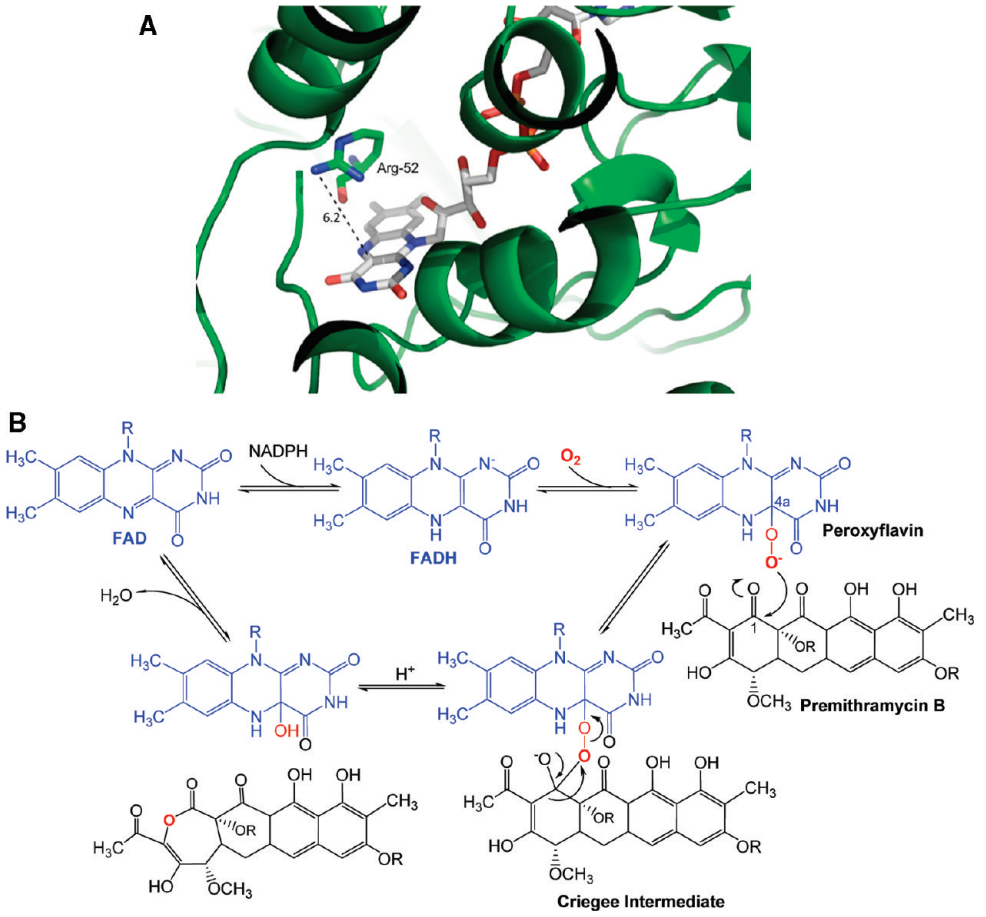

FIGURE 8: (A) View of the catalytically important arginine 52 (R52, green stick, N in blue, O in red) residue of MtmOIV above the flavin ring of FAD (gray stick, N in blue, O in red, P in orange). The measured distance (dotted line) between the N atoms of the guanidine residue of R52 and the flavin ring surface is ~6.2 Å in the shown conformation. The remainder of the enzyme (ribbon) is depicted in green. (B) Suggested Baeyer–Villiger reaction mechanism of the MtmOIV reaction, involving the peroxyflavin and Criegee intermediates. R denotes deoxysugar chains.

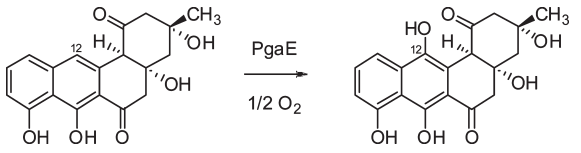

FIGURE 9: PgaE reaction. PgaE is an early acting hydroxylase in the biosynthesis of angucylinone gaudimycin C, catalyzing the 12-hydroxylation of UWM6 (left) to 12-hydroxy-UWM6 (right).

The reactions between the two enzymes do share the oxidative/reductive property provided by the cofactors FAD and NADPH, but the primary reaction is different. Like PgaE, MtmOIV belongs to the *p*-hydroxybenzoate hydroxylase (PHBH) fold family as well as the GR_2 subclass of FAD-dependent enzymes, which previously contained no characterized BVMO (*43*, *69*). Both PgaE and MtmOIV process bulky tetracyclic polyketide-derived substrates in their active site, in contrast to phenylacetone monooxygenase (PAMO) that acts on a relatively small substrate (*33*); however, the MtmOIV substrate is much more complex, because it is highly decorated with deoxysugars, while the PgaE substrate lacks any sugar moiety.

The structure of MtmOIV presented here can now be used to guide mutations that can allow different substrates to access the active site cavity and to be converted potentially into additional active anticancer drug compounds. The generation of analogues MTM SK (*40*), MTM SDK (*20*), and demycarosyl-3D-*β*-D-digitoxosyl-MTM (*41*) (Figure 10), which all possess increased efficacy in some aspects compared to MTM, shows that an improvement of the biological activity of the natural product MTM is realistic.

While MTM SK and MTM SDK differ from MTM with respect to their three-side chain, demycarosyl-3D-*β*-D-digitoxosyl-MTM is an example in which an improvement was achieved through modification of the saccharide pattern, a strategy we want to further exploit but is currently hampered by substrate specificity restrictions of MtmOIV. Demycarosyl-3D-*β*-D-digitoxosyl-MTM was one of only three fully glycosylated MTM analogues with modified sugar moieties that could be generated through combinatorial biosynthesis involving the native MtmOIV. However, it differs from MTM only with respect to the E-sugar moiety, which is D-digitoxose instead of D-mycarose; i.e., it lacks only the 3E-CH_3 residue (Figure 10).

We hoped that the MtmOIV structure would provide clues about how to reengineer the enzyme to accommodate and process premithramycin B analogues with significantly different saccharide patterns, particularly with modified E-sugar moieties, because this terminal sugar of the trisaccharide chain plays a crucial role in MTM's interaction with the DNA (*70*, *71*). The L107A mutant shows that a residue seemingly involved in the binding of the disaccharide chain of the substrate, Leu-107, seems to be crucial in anchoring both the substrate and FAD in the active site, and its mutation to alanine led to loss of FAD binding and loss of activity (Table 2). Interestingly, the here described F89A and R204A mutants showed significantly increased

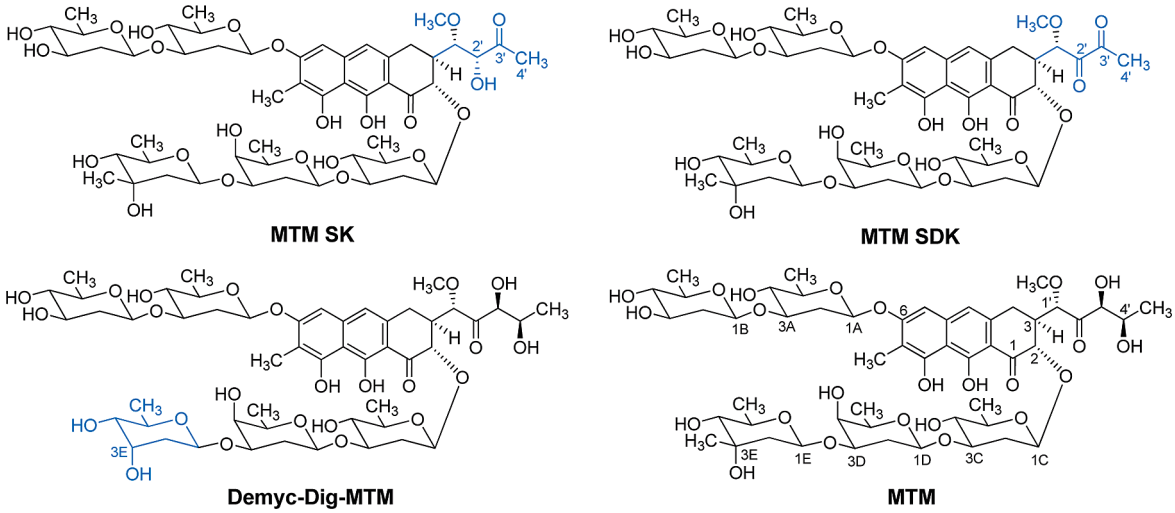

FIGURE 10: Chemical structures of mithramycin (MTM) analogues mithramycin SK (MTM SK) (*40*), mithramycin SDK (MtmSDK) (*20*), and 3D-demycarosyl-3D-digitoxosyl-mithramycin (Demyc-Dig-MTM) (*41*), all generated by combinatorial biosynthesis, which have increased efficacy compared with that of MTM. The structural differences compared with MTM are highlighted in blue.

efficiency versus that of the wild-type enzyme, based on the k_{cat}/K_m values. Thus, both of these bulky residues may be important for the stabilization of the trisaccharide chain of substrate premithramycin B in the substrate binding pocket, interacting particularly with sugar E of this chain. These two mutants show that Phe-89 and Arg-204 in MtmOIV are possibly involved in the substrate specificity of the enzyme binding pocket. This specificity could constrict the binding pocket, designed to house the specific substrate premithramycin B in a biological environment where many possible substrates are present, e.g., premithramycin-type intermediates of the *mtm* pathway that are not yet completely glycosylated (*29*, *72*). However, such specific binding could decrease even the level of binding of the natural substrate, and consequently, reduction of these more bulky residues to a less space-filling alanine residue may in fact relax the binding pocket to allow greater binding of the natural substrate and possible binding of non-natural substrates as well. Consequently, the in vitro kinetic assays exhibit an increased rate of turnover due to a relaxation of the spatial limitations of this binding region in mutants F89A and R204A. Our future work will further focus on using the MtmOIV crystal structure to perform systematic mutagenesis along the substrate binding cavity.

In summary, we presented the crystal structure of MtmOIV, a BVMO catalyzing the key step of the biosynthesis of the anticancer agent mithramycin. Following a useful new classification system (*2*), MtmOIV appears to be an example of an atypical class A flavoprotein monooxygenase catalyzing a Baeyer–Villiger oxidation. The crystal structure provides supporting evidence for a flavin-catalyzed BV reaction involving a peroxyflavin intermediate for its nucleophilic attack, in contrast to typical class A flavoprotein monooxygenases that form a reactive hydroperoxyflavin instead and perform electrophilic attacks. The crystal structure of the atypical BVMO MtmOIV was determined by X-ray crystallography using molecular replacement, for which we took advantage of the crystal structure data of the structurally similar monooxygenase PgaE, a hydroxylase, which is, considering the hydroxylation reaction it catalyzes, a typical class A flavoprotein requiring a hydroperoxyflavin intermediate for its electrophilic aromatic substitution reaction (Figures 1, 8B, and 9). Given the low degree of similarity of MtmOIV with other BVMOs (e.g., only 8% sequence identity with PAMO) and the fact that MtmOIV lacks the typical sequence motif of type I BVMOs and is not related to type II BVMOs (*4*), MtmOIV represents a new class of BVMO.

Using the structural information and substrate modeling results, MtmOIV mutants that support the conclusions drawn regarding the FAD binding and also provide further evidence regarding residues involved in the substrate binding site, which were identified by computational substrate docking experiments, were engineered. The MtmOIV crystal structure may assist in combinatorial biosynthetic efforts to generate new MTM analogues with drastically altered saccharide patterns, since structure-inspired MtmOIV mutants might accommodate different premithramycin-type substrates and convert them into new mithramycin analogues with potentially increased activity or decreased toxicity.

ACKNOWLEDGMENT

We thank the staff at the SER-CAT 22-ID beamline at the Advanced Photon Source for their assistance in data collection. We also thank Professor David W. Rodgers and the University of Kentucky Center for Structural Biology as well as the University of Kentucky Research foundation for their support.

REFERENCES

1. Mihovilovic, M. D., Rudroff, F., Grotzl, B., Kapitan, P., Snajdrova, R., Rydz, J., and Mach, R. (2005) Family clustering of Baeyer-Villiger monooxygenases based on protein sequence and stereopreference. *Angew. Chem., Int. Ed. 44*, 3609–3613.
2. van Berkel, W. J. H., Kamerbeek, N. M., and Fraaije, M. W. (2006) Flavoprotein monooxygenases, a diverse class of oxidative biocatalysts. *J. Biotechnol. 124*, 670–689.
3. Kamerbeek, N. M., Fraaije, M. W., and Janssen, D. B. (2004) Identifying determinants of NADPH specificity in Baeyer-Villiger monooxygenases. *Eur. J. Biochem. 271*, 2107–2116.
4. Kamerbeek, N. M., Janssen, D. B., van Berkel, W. J. H., and Fraaije, M. W. (2003) Baeyer-Villiger Monooxygenases, and Emerging Family of Flavin-Dependent Biocatalysts. *Adv. Synth. Catal. 345*, 667–678.
5. Willetts, A. (1997) Structural studies and synthetic applications of Baeyer-Villiger monooxygenases. *Trends Biotechnol. 15*, 55–62.
6. Hilker, I., Gutierrez, M. C., Furstoss, R., Ward, J., Wohlgemuth, R., and Alphand, V. (2008) Preparative scale Baeyer-Villiger biooxidation at high concentration using recombinant *Escherichia*

coli and in situ substrate feeding and product removal process. *Nat. Protoc. 3*, 546–554.
7. Reetz, M. T., Brunner, B., Schneider, T., Schulz, F., Clouthier, C. M., and Kayser, M. M. (2004) Directed evolution as a method to create enantioselective cyclohexanone monooxygenases for catalysis in Baeyer-Villiger reactions. *Angew. Chem., Int. Ed. 43*, 4075–4078.
8. Ehrlich, K. C., Montalbano, B., Boue, S. M., and Bhatnagar, D. (2005) An aflatoxin biosynthesis cluster gene encodes a novel oxidase required for conversion of versicolorin a to sterigmatocystin. *Appl. Environ. Microbiol. 71*, 8963–8965.
9. Jia, X. Y., Tian, Z. H., Shao, L., Qu, X. D., Zhao, Q. F., Tang, J., Tang, G. L., and Liu, W. (2006) Genetic characterization of the chlorothricin gene cluster as a model for spirotetronate antibiotic biosynthesis. *Chem. Biol. 13*, 575–585.
10. Wright, J. L. C., Hu, T., McLachlan, J. L., Needham, J., and Walter, J. A. (1996) Biosynthesis of DTX-4: Confirmation of a Polyketide Pathway, Proof of a Baeyer-Villiger Oxidation Step, and Evidence for an Unusual Carbon Deletion Process. *J. Am. Chem. Soc. 118*, 8757–8758.
11. Rix, U., Remsing, L. L., Hoffmeister, D., Bechthold, A., and Rohr, J. (2003) Urdamycin L: A novel metabolic shunt product that provides evidence for the role of the *urd*M gene in the urdamycin A biosynthetic pathway of *Streptomyces fradiae* TÜ2717. *ChemBioChem 4*, 109–111.
12. Townsend, C. A., Christensen, S. B., and Davis, S. G. (1982) Bisfuran formation in aflatoxin biosynthesis: The role of versiconal acetate. *J. Am. Chem. Soc. 104*, 6154–6155.
13. Kharel, M. K., Zhu, L., Liu, T., and Rohr, J. (2007) Multi-oxygenase complexes of the gilvocarcin and jadomycin biosyntheses. *J. Am. Chem. Soc. 129*, 3780–3781.
14. Dover, L. G., Corsino, P. E., Daniels, I. R., Cocklin, S. L., Tatituri, V., Besra, G. S., and Futterer, K. (2004) Crystal structure of the TetR/CamR family repressor *Mycobacterium tuberculosis* EthR implicated in ethionamide resistance. *J. Mol. Biol. 340*, 1095–1105.
15. Fraaije, M. W., Kamerbeek, N. M., Heidekamp, A. J., Fortin, R., and Janssen, D. B. (2004) The Prodrug Activator EtaA from *Mycobacterium tuberculosis* Is a Baeyer-Villiger Monooxygenase. *J. Biol. Chem. 279*, 3354–3360.
16. Garbe, L. A., and Tressl, R. (2004) Enzymatic Baeyer-Villiger oxidation as the key step in decano-4-lactone and decano-5-lactone degradation by *Sporobolomyces odorus*. *Chem. Biodiversity 1*, 900–915.
17. Koma, D., Sakashita, Y., Kubota, K., Fujii, Y., Hasumi, F., Chung, S. Y., and Kubo, M. (2004) Degradation pathways of cyclic alkanes in *Rhodococcus* sp. NDKK48. *Appl. Microbiol. Biotechnol. 66*, 92–99.
18. Kataoka, M., Honda, K., Sakamoto, K., and Shimizu, S. (2007) Microbial enzymes involved in lactone compound metabolism and their biotechnological applications. *Appl. Microbiol. Biotechnol. 75*, 257–266.
19. Blume, S. W., Snyder, R. C., Ray, R., Thomas, S., Koller, C. A., and Miller, D. M. (1991) Mithramycin inhibits Sp1 binding and selectively inhibits transcriptional activity of the dihydrofolate reductase gene in vitro and in vivo. *J. Clin. Invest. 88*, 1613–1621.
20. Albertini, V., Jain, A., Vignati, S., Napoli, S., Rinaldi, A., Kwee, I., Nur-e-Alam, M., Bergant, J., Bertoni, F., Carbone, G. M., Rohr, J., and Catapano, C. V. (2006) Novel GC-rich DNA-binding compound produced by a genetically engineered mutant of the mithramycin producer *Streptomyces argillaceus* exhibits improved transcriptional repressor activity: Implications for cancer therapy. *Nucleic Acids Res. 34*, 1721–1734.
21. Bianchi, N., Rutigliano, C., Passadore, M., Tomassetti, M., Pippo, L., Mischiati, C., Feriotto, G., and Gambari, R. (1997) Targeting of the HIV-1 long terminal repeat with chromomycin potentiates the inhibitory effects of a triplex-forming oligonucleotide on Sp1-DNA interactions and in vitro transcription. *Biochem. J. 326*, 919–927.
22. Black, A. R., Black, J. D., and Azizkhan-Clifford, J. (2001) Sp1 and kruppel-like factor family of transcription factors in cell growth regulation and cancer. *J. Cell. Physiol. 188*, 143–160.
23. Gambari, R., Feriotto, G., Rutigliano, C., Bianchi, N., and Mischiati, C. (2000) Biospecific interaction analysis (BIA) of low-molecular weight DNA-binding drugs. *J. Pharmacol. Exp. Ther. 294*, 370–377.
24. Kennedy, B. J., and Torkelson, J. L. (1995) Long-term follow-up of stage III testicular carcinoma treated with mithramycin (plicamycin). *Med. Pediatr. Oncol. 24*, 327–328.
25. Hadjipavlou, A. G., Gaitanis, L. N., Katonis, P. G., and Lander, P. (2001) Paget's disease of the spine and its management. *Eur. Spine J. 10*, 370–384.
26. Pecherstorfer, M., Brenner, K., and Zojer, N. (2003) Current management strategies for hypercalcemia. *Treat. Endocrinol. 2*, 273–292.
27. Ferrante, R. J., Ryu, H., Kubilus, J. K., D'Mello, S., Sugars, K. L., Lee, J., Lu, P., Smith, K., Browne, S., Beal, M. F., Kristal, B. S., Stavrovskaya, I. G., Hewett, S., Rubinsztein, D. C., Langley, B., and Ratan, R. R. (2004) Chemotherapy for the brain: The antitumor antibiotic mithramycin prolongs survival in a mouse model of Huntington's disease. *J. Neurosci. 24*, 10335–10342.
28. Rohr, J., Mendez, C., and Salas, J. (1999) The Biosynthesis of Aureolic Acid Group Antibiotics. *Bioorg. Chem. 27*, 41–54.
29. Nur-e-Alam, M., Méndez, C., Salas, J. A., and Rohr, J. (2005) Elucidation of the glycosylation sequence of mithramycin biosynthesis: Isolation of 3A-deolivosylpremithramycin B and its conversion to premithramycin B by glycosyltransferase MtmGII. *ChemBioChem 6*, 632–636.
30. Prado, L., Fernandez, E., Weissbach, U., Blanco, G., Quiros, L. M., Brana, A. F., Mendez, C., Rohr, J., and Salas, J. A. (1999) Oxidative cleavage of premithramycin B is one of the last steps in the biosynthesis of the antitumor drug mithramycin. *Chem. Biol. 6*, 19–30.
31. Gibson, M., Nur-e-Alam, M., Lipata, F., Oliveira, M. A., and Rohr, J. (2005) Characterization of Kinetics and Products of the Baeyer-Villiger Oxygenase MtmOIV, the Key Enzyme of the Biosynthetic Pathway toward the Natural Product Anticancer Drug Mithramycin from *Streptomyces argillaceus*. *J. Am. Chem. Soc. 127*, 17594–17595.
32. Isupov, M. N., and Lebedev, A. A. (2008) NCS-constrained exhaustive search using oligomeric models. *Acta Crystallogr. D64*, 90–98.
33. Malito, E., Alfieri, A., Fraaije, M. W., and Mattevi, A. (2004) Crystal structure of a Baeyer-Villiger monooxygenase. *Proc. Natl. Acad. Sci. U.S.A. 101*, 13157–13162.
34. Van Beilen, J. B., Mourlane, F., Seeger, M. A., Kovac, J., Li, Z., Smits, T. H., Fritsche, U., and Witholt, B. (2003) Cloning of Baeyer-Villiger monooxygenases from *Comamonas*, *Xanthobacter* and *Rhodococcus* using polymerase chain reaction with highly degenerate primers. *Environ. Microbiol. 5*, 174–182.
35. Morii, S., Sawamoto, S., Yamauchi, Y., Miyamoto, M., Iwami, M., and Itagaki, E. (1999) Steroid monooxygenase of *Rhodococcus rhodochrous*: Sequencing of the genomic DNA, and hyperexpression, purification, and characterization of the recombinant enzyme. *J. Biochem. 126*, 624–631.
36. Rodriguez, D., Quiros, L. M., Braña, A. F., and Salas, J. A. (2003) Purification and characterization of a monooxygenase involved in the biosynthetic pathway of the antitumor drug mithramycin. *J. Bacteriol. 185*, 3962–3965.
37. Wang, C., Gibson, M., Rohr, J., and Oliveira, M. A. (2005) Crystallization and X-ray diffraction properties of Baeyer-Villiger monooxygenase MtmOIV from the mithramycin biosynthetic pathway in *Streptomyces argillaceus*. *Acta Crystallogr. F61*, 1023–1026.
38. Prado, L., Fernandez, E., Weissbach, U., Blanco, G., Quiros, L. M., Brana, A. F., Méndez, C., Rohr, J., and Salas, J. A. (1999) Oxidative cleavage of premithramycin B is one of the last steps in the biosynthesis of the antitumor drug mithramycin. *Chem. Biol. 6*, 19–30.
39. Remsing, L. L., Bahadori, H. R., Carbone, G. M., McGuffie, E. M., Catapano, C. V., and Rohr, J. (2003) Inhibition of c-src transcription by mithramycin: Structure-activity relationships of biosynthetically produced mithramycin analogues using the c-src promoter as target. *Biochemistry 42*, 8313–8324.
40. Remsing, L. L., Gonzalez, A. M., Nur-e-Alam, M., Fernandez-Lozano, M. J., Braña, A. F., Rix, U., Oliveira, M. A., Méndez, C., Salas, J. A., and Rohr, J. (2003) Mithramycin SK, a novel antitumor drug with improved therapeutic index, mithramycin SA, and demycarosylmithramycin SK: Three new products generated in the mithramycin producer *Streptomyces argillaceus* through combinatorial biosynthesis. *J. Am. Chem. Soc. 125*, 5745–5753.
41. Baig, I., Pérez, M., Braña, A. F., Gomathinayagam, R., Damodaran, C., Salas, J. A., Méndez, C., and Rohr, J. (2008) Mithramycin analogues generated by combinatorial biosynthesis show improved bioactivity. *J. Nat. Prod. 71*, 199–207.
42. Pérez, M., Baig, I., Braña, A. F., Salas, J. A., Rohr, J., and Méndez, C. (2008) Generation of new derivatives of the antitumor antibiotic mithramycin by altering the glycosylation pattern through combinatorial biosynthesis. *ChemBioChem 9*, 2295–2304.
43. Dym, O., and Eisenberg, D. (2001) Sequence-structure analysis of FAD-containing proteins. *Protein Sci. 10*, 1712–1728.
44. Koskiniemi, H., Metsa-Ketela, M., Dobritzsch, D., Kallio, P. Korhonen, H., Mantsala, P., Schneider, G., and Niemi, J. (2007) Crystal structures of two aromatic hydroxylases involved in the early tailoring steps of angucycline biosynthesis. *J. Mol. Biol. 372*, 633–648.
45. Otwinowski, Z., and Minor, W. (1997) Processing of X-Ray Diffraction Data Collected in Oscillation Mode. *Methods Enzymol. 276* 538–557.
46. Collaborative Computational Project, No. 4 (1994) The CCP4 suite: Programs for protein crystallography. *Acta Crystallogr. D50*, 760–763.

47. Thompson, J. D., Higgins, D. G., and Gibson, T. J. (1994) CLUSTAL W: Improving the sensitivity of progressive multiple sequence alignment through sequence weighting, position-specific gap penalties and weight matrix choice. *Nucleic Acids Res. 22*, 4673–4680.
48. Stein, N. (2008) CHAINSAW: A program for mutating pdb files used as templates in molecular replacement. *J. Appl. Crystallogr. 41*, 641–643.
49. Adams, P. D., Grosse-Kunstleve, R. W., Hung, L. W., Ioerger, T. R., McCoy, A. J., Moriarty, N. W., Read, R. J., Sacchettini, J. C., Sauter, N. K., and Terwilliger, T. C. (2002) PHENIX: Building new software for automated crystallographic structure determination. *Acta Crystallogr. D58*, 1948–1954.
50. Emsley, P., and Cowtan, K. (2004) Coot: Model-building tools for molecular graphics. *Acta Crystallogr. D60*, 2126–2132.
51. Brunger, A. T., Adams, P. D., Clore, G. M., DeLano, W. L., Gros, P., Grosse-Kunstleve, R. W., Jiang, J. S., Kuszewski, J., Nilges, M., Pannu, N. S., Read, R. J., Rice, L. M., Simonson, T., and Warren, G. L. (1998) Crystallography & NMR system: A new software suite for macromolecular structure determination. *Acta Crystallogr. D54*, 905–921.
52. Davis, I. W., Murray, L. W., Richardson, J. S., and Richardson, D. C. (2004) MOLPROBITY: Structure validation and all-atom contact analysis for nucleic acids and their complexes. *Nucleic Acids Res. 32*, W615–W619.
53. Delano, W. L. (2002) *The PyMOL Molecular Graphics System*, DeLano Scientific, San Carlos, CA.
54. Gille, C., and Frommel, C. (2001) STRAP: Editor for STRuctural Alignments of Proteins. *Bioinformatics 17*, 377–378.
55. Wang, W., and Malcolm, B. A. (2002) Two-stage polymerase chain reaction protocol allowing introduction of multiple mutations, deletions, and insertions, using QuikChange site-directed mutagenesis. *Methods Mol. Biol. 182*, 37–43.
56. Bachmann, H. S., Siffert, W., and Frey, U. H. (2003) Successful amplification of extremely GC-rich promoter regions using a novel 'slowdown PCR' technique. *Pharmacogenetics 13*, 759–766.
57. Jameson, G. N., Jin, W., Krebs, C., Perreira, A. S., Tavares, P., Liu, X., Theil, E. C., and Huynh, B. H. (2002) Stoichiometric production of hydrogen peroxide and parallel formation of ferric multimers through decay of the diferric-peroxo complex, the first detectable intermediate in ferritin mineralization. *Biochemistry 41*, 13435–13443.
58. Holt, A., Sharman, D. F., Baker, G. B., and Palcic, M. M. (1997) A continuous spectrophotometric assay for monoamine oxidase and related enzymes in tissue homogenates. *Anal. Biochem. 244*, 384–392.
59. Schuettelkopf, A. W., and van Aalten, D. M. F. (2004) PRODRG: A tool for high-throughput crystallography of protein-ligand complexes. *Acta Crystallogr. D60*, 1355–1363.
60. van Aalten, D. M., Bywater, R., Findlay, J. B., Hendlich, M., Hooft, R. W., and Vriend, G. (1996) PRODRG, a program for generating molecular topologies and unique molecular descriptors from coordinates of small molecules. *J. Comput.-Aided Mol. Des. 10*, 255–262.
61. Goodsell, D. S., Morris, G. M., and Olson, A. J. (1996) Automated docking of flexible ligands: Applications of AutoDock. *J. Mol. Recognit. 9*, 1–5.
62. Wallace, A. C., Laskowski, R. A., and Thornton, J. M. (1995) LIGPLOT: A program to generate schematic diagrams of protein-ligand interactions. *Protein Eng. 8*, 127–134.
63. Ryan, K. S., Chakraborty, S., Howard-Jones, A. R., Walsh, C. T., Ballou, D. P., and Drennan, C. L. (2008) The FAD cofactor of RebC shifts to an IN conformation upon flavin reduction. *Biochemistry 47*, 13506–13513.
64. Krissinel, E., and Henrick, K. (2007) Inference of macromolecular assemblies from crystalline state. *J. Mol. Biol. 372*, 774–797.
65. Morris, G. M., Goodsell, D. S., Halliday, R. S., Huey, R., Hart, W. E., Belew, R. K., and Olson, A. J. (1998) Automated Docking Using a Lamarckian Genetic Algorithm and an Empirical Binding Free Energy Function. *J. Comput. Chem. 19*, 1639–1662.
66. Ryan, K. S., Howard-Jones, A. R., Hamill, M. J., Elliott, S. J., Walsh, C. T., and Drennan, C. L. (2007) Crystallographic trapping in the rebeccamycin biosynthetic enzyme RebC. *Proc. Natl. Acad. Sci. U.S.A. 104*, 15311–15316.
67. Torres Pazmino, D. E., Baas, B.-J., Janssen, D. B., and Fraaije, M. W. (2008) Kinetic Mechanism of Phenylacetone Monooxygenase from *Thermobifida fusca*. *Biochemistry 47*, 4082–4093.
68. Kallio, P., Liu, Z., Mantsala, P., Niemi, J., and Metsa-Ketela, M. (2008) Sequential action of two flavoenzymes, PgaE and PgaM, in angucycline biosynthesis: Chemoenzymatic synthesis of gaudimycin C. *Chem. Biol. 15*, 157–166.
69. Mattevi, A. (1998) The PHBH fold: Not only flavoenzymes. *Biophys. Chem. 70*, 217–222.
70. Sastry, M., Fiala, R., and Patel, D. J. (1995) Solution structure of mithramycin dimers bound to partially overlapping sites on DNA. *J. Mol. Biol. 251*, 674–689.
71. Sastry, M., and Patel, D. J. (1993) Solution structure of the mithramycin dimer-DNA complex. *Biochemistry 32*, 6588–6604.
72. Fernandez, E., Weissbach, U., Sanchez Reillo, C., Braña, A. F., Méndez, C., Rohr, J., and Salas, J. A. (1998) Identification of two genes from *Streptomyces argillaceus* encoding glycosyltransferases involved in transfer of a disaccharide during biosynthesis of the antitumor drug mithramycin. *J. Bacteriol. 180*, 4929–4937.